Scalable Computations of Wasserstein Barycenter via Input Convex Neural Networks

Jiaojiao Fan [1] **Amirhossein Taghvaei** [2] **Yongxin Chen** [1]

Abstract

Wasserstein Barycenter is a principled approach to represent the weighted mean of a given set of probability distributions, utilizing the geometry induced by optimal transport. In this work, we present a novel scalable algorithm to approximate the Wasserstein Barycenters aiming at high-dimensional applications in machine learning. Our proposed algorithm is based on the Kantorovich dual formulation of the Wasserstein-2 distance as well as a recent neural network architecture, input convex neural network, that is known to parametrize convex functions. The distinguishing features of our method are: i) it only requires samples from the marginal distributions; ii) unlike the existing approaches, it represents the Barycenter with a generative model and can thus generate infinite samples from the barycenter without querying the marginal distributions; iii) it works similar to Generative Adversarial Model in one marginal case. We demonstrate the efficacy of our algorithm by comparing it with the state-of-art methods in multiple experiments. [1]

1. Introduction

The Wasserstein barycenter is concerned with the (weighted) average of multiple given probability distributions. It is based on the natural geometry over the space of distributions induced by optimal transport (Villani, 2003) theory and serves as a counterpart of arithmetic mean/average for data of distribution-type. Compared to other methods, Wasserstein barycenter provides a principled approach to average probability distributions, fully utilizing the underlying geometric structure of the data (Agueh & Carlier, 2011). During the past few years, it has found applications in several machine learning problems. For instance, in sensor fusion, Wasserstein barycenter is used to merge/average datasets collected from multiple sensors to generate a single collective result (Elvander et al., 2018). The advantage of Wasserstein barycenter is its ability to preserves the modality of the different datasets, a highly desirable property in practice (Jiang et al., 2012). Wasserstein Barycenter has also been observed to be effective in removing batch effects of the sensor measurements (Yang & Tabak, 2019). It has also found application in large scale Bayesian inference for averaging the results from Markov chain Monte Carlo (MCMC) Bayesian inference carried out over subsets of the observations (Srivastava et al., 2015; Staib et al., 2017; Srivastava et al., 2018). It has also been useful in image processing for texture mixing (Rabin et al., 2011) and shape interpolation (Solomon et al., 2015).

The bottleneck of utilizing Wasserstein barycenter in machine learning applications remains to be computational. Indeed, when the data is discrete, namely, the given probability distributions are over discrete space (e.g., grid), the Wasserstein barycenter problem can be solved using linear programming (Anderes et al., 2016). This has been greatly accelerated by introducing an entropy term (Cuturi & Doucet, 2014, Algorithm 1) (Solomon et al., 2015) as in Sinkhorn algorithm (Cuturi, 2013). However, these methods are not suitable for many machine learning applications involving distributions over continuous space. First of all, it requires discretization of the distribution to implement these methods and thus doesn't scale to high dimensional settings. Secondly, in some applications such as MCMC Bayesian inference (Andrieu et al., 2003; Srivastava et al., 2018) the explicit formulas of the distributions are not accessible, which precludes these discretization-based algorithms. When the support atoms are free to move, there are algorithms that interchangeably optimize the support weights and locations (Cuturi & Doucet, 2014, Algorithm 2) (Luise et al., 2019; Altschuler & Boix-Adsera, 2021) which can also be formulated in stochastic optimization framework (Claici et al., 2018). But these free-support methods become computationally highly expensive when the number of support points is large.

[1]Georgia Institute of Technology [2]University of California, Irvine. Correspondence to: Yongxin Chen <yongchen@gatech.edu>.

Proceedings of the 38^{th} International Conference on Machine Learning, PMLR 139, 2021.

[1]Download Code at https://github.com/sbyebss/Scalable-Wasserstein-Barycenter

Contribution: We propose a computationally efficient and scalable algorithm for estimating the Wasserstein barycenter of probability distributions over continuous spaces. Our method is based on a Kantorovich-type dual characterization of the Wasserstein barycenter, which involves optimization over convex functions, and the recently introduced input convex neural networks (ICNN) (Amos et al., 2017; Chen et al., 2018b), that provides powerful representation of convex functions. Remarkably, in our framework, the (weighted) barycenter is represented by a generator network (Goodfellow et al., 2014; Arjovsky et al., 2017), that allows characterization of continuous distributions and fast and unlimited sampling from barycenter. We prove the consistency of our formulation in Proposition 1, and demonstrate its performance and its scaling properties in truly high-dimensional setting through extensive evaluations over various benchmark experiments including synthetic and real data-set and provide comparisons with several state-of-art algorithms: Korotin et al. (2021b), Li et al. (2020), Cuturi & Doucet (2014). Our experiments reveal significant improvement in estimating the barycenter in high-dimensional setting compared to most existing algorithms. We also showcase the the ability of our method to perform as a generative adversarial network (GAN) in the one marginal case and propose a heuristic extension to learn barycenter of arbitrary weights through a single training process.

Related work: Our proposed algorithm is closely related to continuous Wasserstein barycenter proposed by Li et al. (2020) and Korotin et al. (2021b). Similar to our approach, both of them are based on dual formulation of the Wasserstein barycenter problem and representing the potential functions with neural networks. However, the approach in Li et al. (2020) does not restrict the potential functions to be convex. Instead, an entropic or l_2 regularization term is added to ensure that the optimal potential functions are approximately convex. The addition of the regularization term introduces undesirable bias error which becomes severe in high-dimensional problems as shown in Figure 5-6 and also reported in (Korotin et al., 2021b, Table1-4) (Li et al., 2020, Section 5). The approach in Korotin et al. (2021b) restricts the potentials to be convex using ICNN, however, it includes a cycle regularizer term to ensure the potential functions are dual conjugate. Their formulation also involves a congruence regularizer to guarantee that the optimal potential functions are consistent with the true barycenter. The congruence regularizer requires selection of a priory probability distribution that is bounded below by the true barycenter, which is a non-trivial task. Moreover, the addition of the regularization terms distorts the nice optimization landscape of the original problem. The problem may become non-convex even for the simple setting of restriction to quadratic functions (see Sec. G in supplementary material). In contrast, our formulation does not involve additional regularization terms and retains the optimization landscape of the original problem. Moreover, a distinct feature of our algorithm is representing the barycenter using a generative model which allows a low-dimensional representation of the barycenter and access to infinitely many samples, while both of these methods represent the barycenter using the Monge maps from the marginals, and limits the number of samples to the number available from marginal distributions.

Earlier stochastic Wasserstein barycenter method (Claici et al., 2018) also aims at calculating barycenters for continuous distributions using samples. However, they adopt a semi-discrete approach that models the barycenter with a finite set of points. That is, even though the marginals are continuous, the barycenter is discrete. Several other sample-based algorithms (Staib et al., 2017; Kuang & Tabak, 2019; Mi et al., 2020) are also of semi-discrete-type. Most other Wasserstein barycenter algorithms are for discrete distributions and require discretization if applied to continuous distributions. An incomplete list includes (Cuturi & Doucet, 2014; Benamou et al., 2015; Solomon et al., 2015).

The subject of this work is also related to the vast amount of literature on estimating the optimal transport map and Wasserstein distance (see (Peyré et al., 2019) for a complete list). Closely related to this paper are the recent works that aim to extend the optimal transport map estimation to large-scale machine learning settings (Genevay et al., 2016; Seguy et al., 2017; Liu et al., 2018; Chen et al., 2018a; Leygonie et al., 2019; Xie et al., 2019). In particular, our algorithm is inspired by the recent advances in estimation of optimal transport map and Wasserstein-2 distance using ICNNs (Taghvaei & Jalali, 2019; Makkuva et al., 2020; Korotin et al., 2021a).

2. Background

2.1. Optimal transport and Wasserstein distance

Given two probability distributions ν, μ over Euclidean space $\mathbb{R}^n$ with finite second moments, the optimal transport (Villani, 2003) (OT) problem with quadratic unit cost seeks an optimal joint distribution of ν, μ that minimizes the total transport cost. More specifically, it is formulated as $W_2^2(\nu, \mu) := \min_{\pi \in \Pi(\nu,\mu)} \int_{\mathbb{R}^n \times \mathbb{R}^n} \|x - y\|^2 d\pi(x, y)$, where $\Pi(\nu, \mu)$ denotes the set of all joint distributions of ν and μ. The square-root of the minimum transport cost defines the celebrated Wasserstein-2 distance W_2, which is known to enjoy many nice geometrical properties compared to other distances for distributions (Ambrosio et al., 2008).

The Kantorovich dual of the OT problem reads

$$\frac{1}{2}W_2^2(\nu, \mu) = \sup_{(\phi,\psi)\in\Phi} \mathbb{E}_\nu[\phi(X)] + \mathbb{E}_\mu[\psi(Y)], \quad (1)$$

where $\Phi := \{(\phi, \psi) \in L^1(\nu) \times L^1(\mu)\,;\, \phi(x) + \psi(y) \leq$

$\frac{1}{2}\|x-y\|^2,\ \ \forall x, y\}$. Let $f(x) = \|x\|^2/2 - \phi(x)$, then (1) can be rewritten as

$$\frac{1}{2}W_2^2(\nu,\mu) = C_{\nu,\mu} - \inf_{f\in\textbf{CVX}}\{\mathbb{E}_\nu[f(X)] + \mathbb{E}_\mu[f^*(Y)]\} \quad (2)$$

where **CVX** stands for the set of convex functions, $C_{\nu,\mu} := (1/2)\{\mathbb{E}_\nu[\|X\|^2] + \mathbb{E}_\mu[\|Y\|^2]\}$, and the f^* is the convex conjugate (Rockafellar, 1970) function of f. The formulation (2) is known as the semi-dual formulation of OT. The **CVX** condition restricts the search space for f which becomes handy for design of optimization algorithms.

Remark 1 *When both of the marginal distributions have densities, Brenier' Theorem gives that ∇f^* is the optimal transport map from μ to ν (Villani, 2003) and ∇f is the optimal map from ν to μ.*

2.2. Wasserstein Barycenter

Wasserstein barycenter is OT-based average of probability distributions. Given a set of probability distributions μ_i, $i = 1, 2, \ldots, N$ and a weight vector $a \in \mathbb{R}^N$ ($a_i \geq 0$, $i = 1, 2, \ldots, N$ and $\sum_{i=1}^N a_i = 1$), the associated Wasserstein barycenter is defined as the minimizer of

$$\min_\nu \sum_{i=1}^N a_i W_2^2(\nu, \mu_i). \quad (3)$$

The barycenter problem (3) can be reformulated as a linear programming (Agueh & Carlier, 2011). However, the linear programming-base algorithms don't scale well for high dimensional problems. A special case that can be solved efficiently is when the marginal distributions $\{\mu_i\}$ are Gaussian. Denote the mean and covariance of μ_i as m_i and Σ_i respectively, then their Wasserstein barycenter is a Gaussian distribution with mean being $m = \sum_{i=1}^N a_i m_i$ and covariance Σ being the unique solution to the fixed-point equation $\Sigma = \sum_{i=1}^N a_i(\Sigma^{1/2}\Sigma_i\Sigma^{1/2})^{1/2}$. In Álvarez-Esteban et al. (2016), a simple however efficient algorithm was proposed to solve for Σ.

2.3. Input Convex Neural Network

Input Convex Neural Network (ICNN) is a type of deep neural networks architecture that characterize convex functions (Amos et al., 2017). A fully ICNN (FICNN) leads to a function that is convex with respect to all inputs.

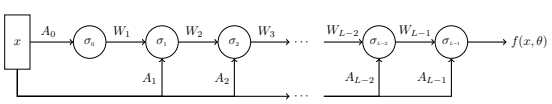

Figure 1: Fully input convex neural network (FICNN)

The FICNN architecture is shown in Fig. 1. It is a L-layer feedforward neural network propagating following, for $l = 0, 1, \ldots, L-1$

$$z_{l+1} = \sigma_l(W_l z_l + A_l x + b_l), \quad (4)$$

where $\{W_l\}, \{A_l\}$ are weight matrices (with the convention that $W_0 = 0$), $\{b_l\}$ are the bias terms, and σ_l denotes the entry-wise activation function at the layer l. Denote the total set of parameters by $\theta = (\{W_l\}, \{A_l\}, \{b_l\})$, then this network defines a map from input x to $f(x;\theta) = z_L$. This map $f(x;\theta)$ is convex in x provided 1) $W_{1:L-1}$ are non-negative; 2) $\sigma_{0:L-1}$ are convex; 3) $\sigma_{1:L-1}$ are non-decreasing (Makkuva et al., 2020). We remark that FICNN has the ability to approximate any convex function over a compact domain with a desired accuracy (Chen et al., 2018b), which makes FICNN an ideal candidate for modeling convex functions.

3. Methods and algorithms

We study the Wasserstein barycenter problem (3) for a given set of marginal distributions $\{\mu_i;\ i = 1, \ldots, N\}$. We consider the setting where the analytic forms of the marginals are not available. Instead, we only have access to independent samples from them. It can be either the cases where a fix set of samples is provided as in supervised learning, or the cases where one can keep sampling from the marginals like in the MCMC Bayesian (Srivastava et al., 2018). Our goal is to recover the true continuous Barycenter ν.

3.1. Deriving the dual problem over convex functions

For a fixed ν, the objective function of (3) is simply a (scaled) summation of the Wasserstein cost between ν and μ_i. Thus, we utilize the semi-dual formulation (2) of OT to evaluate the objective function of (3). However, convex conjugate function f^* is not available explicitly in most of applications, thus we characterize it as

$$f^*(y) = \sup_{g\in\textbf{CVX}} \langle y, \nabla g(y)\rangle - f(\nabla g(y)) \quad (5)$$

with the maximum being achieved at $g = f^*$, the semi-dual formulation (2) can be rewritten as

$$\frac{1}{2}W_2^2(\nu,\mu) = \sup_{f\in\textbf{CVX}} \inf_{g\in\textbf{CVX}} \mathcal{V}_{\nu,\mu}(f,g) + C_{\nu,\mu}, \quad (6)$$

where $\mathcal{V}_{\nu,\mu}(f,g)$ is a functional of f and g defined as

$$\mathcal{V}_{\nu,\mu}(f,g) = -\mathbb{E}_\nu[f(X)] - \mathbb{E}_\mu[\langle Y, \nabla g(Y)\rangle - f(\nabla g(Y))]. \quad (7)$$

This formulation (6) has been utilized in conjugation with FICNN to solve OT problem in (Makkuva et al., 2020) and proved to be advantageous.

Plugging (6) into the Wasserstein barycenter problem (3), we obtain the following reformulation

$$\min_\nu \sum_{i=1}^N a_i \left\{ \sup_{f_i\in\textbf{CVX}} \inf_{g_i\in\textbf{CVX}} \mathcal{V}_{\nu,\mu_i}(f_i, g_i) + C_{\nu,\mu_i} \right\}. \quad (8)$$

Note that we have used different functions (f_i, g_i) to estimate $W_2^2(\nu, \mu_i)$. The first minimization is over all the possible probability distributions to search for the Wasserstein barycenter. This min-max-min formulation enjoys the following property, whose proof is in the supplementary material.

Proposition 1 *When all the marginal distributions μ_i are absolutely continuous with respect to the Lebesgue measure, the unique Wasserstein barycenter $\nu^\star$ of them solves (8). Moreover, the corresponding optimal $f_i^\star$ is the optimal potential in (2) associated with marginals $\nu^\star$ and μ_i.*

Remark 2 *Obtaining convergence rate for first-order optimization algorithms solving (8) is challenging even in the ideal setting that the optimization is carried out in the space of probability distributions. The difficulty arises because of the optimization over ν. While the inner optimization over f_i and g_i are concave and convex respectively, the optimization over ν is not convex. Precisely, it is not geodesically convex on the space of probability distributions equipped with Wasserstein-2 metric (Ambrosio et al., 2008). However, it is possible to obtain guarantees in a restricted setting by establishing a Polyak- Lojasiewicz type inequality. In particular, assuming all μ_i are Gaussian with positive-definite covariance matrices, the gradient-descent algorithm admits a linear convergence rate (Chewi et al., 2020).*

3.2. Solving the barycenter problem

Consider the Wasserstein barycenter problem for a fixed weight vector a. Following (Makkuva et al., 2020) we use FICNN architecture to represent convex functions f_i and g_i. We now use a generator h to model the distribution ν, by transforming samples from a simple distribution η (e.g., Gaussian, uniform) to a complicated distribution, thereby we recover a continuous Barycenter distribution. Thus, using this network parametrization and discarding constant terms, we arrive at the following optimization problem

$$\min_{h} \sup_{f_i \in \textbf{FICNN}} \inf_{g_i \in \textbf{FICNN}} \frac{1}{2}\mathbb{E}_\eta[\|h(Z)\|^2] + \sum_{i=1}^{N} a_i \overline{\mathcal{V}}_{\eta,\mu_i}(f_i, g_i), \tag{9}$$

where $\overline{\mathcal{V}}_{\eta,\mu_i}(f, g)$ is defined as

$$-\mathbb{E}_\eta[f_i(h(Z))] - \mathbb{E}_{\mu_i}[\langle Y^i, \nabla g_i(Y^i)\rangle - f_i(\nabla g_i(Y^i))].$$

We propose Neural Wasserstein Barycenter (NWB) algorithm (Algorithm 1) to solve this three-loop min-max-min problem by alternatively updating h, f_i and g_i using stochastic optimization algorithms. This pipeline is illustrated by the block diagram (Figure 2). We remark that the objective function in (9) can be estimated using samples from μ_i, η. Thus, we just need access to the samples generated by the marginal distributions μ_i instead of their analytic form to compute their Wasserstein barycenter. In practice, we found it more effective to replace the convexity constraints for g_i with a convexity penalty, that is, the negative values of the weight matrices W_l in FICNN (4).

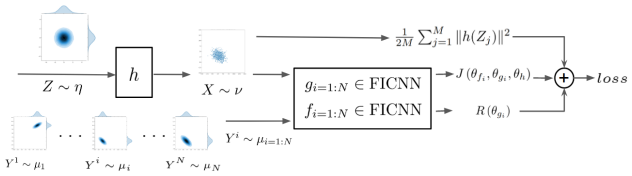

Figure 2: Block diagram for our neural Wasserstein barycenter (NWB) algorithm

Denoting the parameters of h, f_i, g_i by $\theta_h, \theta_{f_i}, \theta_{g_i}$ respectively and the batch size by M, we arrive at the batch estimation of the objective

$$\sum_{i=1}^{N} a_i \left[J(\theta_{f_i}, \theta_{g_i}, \theta_h) + R\left(\theta_{g_i}\right)\right] + \frac{1}{2M}\sum_{j=1}^{M} ||h(Z_j)||^2, \tag{10}$$

where $J\left(\theta_{f_i}, \theta_{g_i}, \theta_h\right)$ represents

$$\frac{1}{M}\sum_{j=1}^{M} f_i\left(\nabla g_i\left(Y_j^i\right)\right) - \left\langle Y_j^i, \nabla g_i\left(Y_j^i\right)\right\rangle - f_i\left(h(Z_j)\right),$$

$R\left(\theta_{g_i}\right) = \lambda \sum_{W_l \in \theta_{g_i}} \|\max\left(-W_l, 0\right)\|_F^2$, Y_j^i represents the j^{th} sample generated by μ_i, $\{Z_j\}$ are samples from η, and $\lambda > 0$ is a hyper-parameter weighing the intensity of regularization.

Algorithm 1 can be extended to obtain the barycenters for all weights in one shot. This extension is included in Sec. B of the supplementary material.

Remark 3 *It is tempting to combine the two minimization steps over h and g_i into one and reduce (9) into a min-max saddle point problem. The resulting algorithm only alternates between f_i updates and h, g_i updates instead of the three-way alternating in Algorithm 1. However, in our implementations, we observed that this strategy is unstable.*

Computation complexity For our algorithm, as well as the algorithms recently proposed in (Korotin et al., 2021b; Li et al., 2020), the computational complexity per iteration scales with $O(NMp)$ where N is the number of marginals, M is the batch-size, and p is the size of the network (the size of network scales almost linearly with dimension d). This should be compared with $O(NMK)$ for Claici et al. (2018) where K is the size of the support for barycenter, and $O(NnK)$ for Cuturi & Doucet (2014) where n is the number of samples of the marginals. Although the size of the network is large, our approach is favored for large scale

Algorithm 1 Neural Wasserstein Barycenter (NWB)

Input: Marginal dist. $\mu_{1:N}$, Generator dist. η, Batch size M
for $k_3 = 1, \dots, K_3$ **do**
  Sample batch $\{Z_j\}_{j=1}^M \sim \eta$
  Sample batch $\left\{Y_j^i\right\}_{j=1}^M \sim \mu_i$ for all $i = 1, \cdots, N$
  for $k_2 = 1, \dots, K_2$ **do**
    for $k_1 = 1, \dots, K_1$ **do**
      Update all θ_{g_i} to decrease (10)
    end for
    Update all θ_{f_i} to increase (10)
    Clip: $W_l = \max(W_l, 0)$ for all θ_{f_i}
  end for
  Update θ_h to decrease (10)
end for

problems where the number of samples n and the dimension d are large (the number of atoms required to approximate a density scales exponentially with dimension).

3.3. Recovering the barycenter

Once Algorithm 1 converges, there are two distinct approaches to recover the Wasserstein barycenter: one through h and one through g_i.

Generative model $h_\sharp\eta$: In our problem formulation (9), the barycenter center is modeled by $h(Z)$ where Z is sampled from a simple distribution η. That is, the barycenter ν is the pushforward of η through the map h, denoted by $h_\sharp\eta$. Once the optimal h is obtained, we can easily sample from the barycenter by sampling Z_j from η and apply the map $h(Z_j)$.

Pushforward map $\nabla g_i \sharp \mu_i$: An alternative method to recover the barycenter is based on the fact, once Algorithm 1 converges, the pair (f_i, g_i) solves the OT problem (6) between the barycenter ν and the marginal μ_i. As mentioned in Remark 1, ∇f^* is the optimal map from marginal distribution to the barycenter. Moreover, the optimal g_i is achieved at $g = f^*$. Hence, the pushforward of μ_i through map ∇g_i is the barycenter. Thus, to sample from the barycenter, we can sample Y_j^i from a marginal and then apply map $\nabla g_i(Y_j^i)$. Note that this approach cannot generate more samples than those are already available in the marginals.

3.4. Barycenter serving as GAN

In case where there is only one marginal distribution, that is, $N = 1$ in (9), Algorithm 1 can be viewed as a type of generative adversarial network (GAN). More specifically, when $N = 1$, the barycener ν coincides with the marginal distribution μ_1. Given samples $\{Y_1^j\}$ from the marginal μ_1, Algorithm 1 produces a generative model $h(Z)$ whose distribution matches the marginal μ_1. Note that one can easily sample using $h(Z)$ and get samples that do not exist in the training data $\{Y_1^j\}$.

In fact, when $N = 1$, Algorithm 1 works very much like a Wasserstein Generative Adversarial Network (WGAN) which leverages the Wasserstein distance to distinguish fake and real samples in GAN. The original WGAN (Arjovsky et al., 2017) is based on the dual formulation for the Wasserstein-1 distance W_1. A heuristic weight clipping (Arjovsky et al., 2017) technique is used to enforce the Lipschitz condition on the potential function in the dual formulation. The WGAN was later improved in WGAN-GP (Gulrajani et al., 2017) via adding a gradient penalty term to promote the Lipschitz condition. From this point of view, Algorithm 1 provides an alternative way to train the generative model with Wasserstein-2 metric (c.f. Leygonie et al. (2019); Korotin et al. (2021a); Salimans et al. (2018); Genevay et al. (2018)).

4. Experiments

In Section 4.1, we present numerical experiments on 2D/3D datasets which serve as proof of concept and qualitatively illustrate the performance of our approach. In Section 4.2, we numerically study the effects of dimensionality and demonstrate the scalability of our algorithms to high-dimensional problems. In Section 4.3 and 4.4, we apply our algorithm in tasks such as Bayesian inference with large scale dataset and color transfer. In Section 4.5, we illustrate the ability of our algorithm to serve as a generative model. The implementation details and further experiments are included in the supplementary materials.

For comparison, we choose the following state of the art algorithms: (i) fast free-support Wasserstein barycenter (CDWB) (Cuturi & Doucet, 2014, Section 4.4); (ii) continuous Wasserstein barycenter without minimax optimization (CWB) (Korotin et al., 2021b); (iii) continuous regularized Wasserstein barycenter (CRWB) (Li et al., 2020). CWB and CRWB involve optimization over N pairs of potentials $\{f_i, g_i\}$ as in NWB, and recover barycenter through $\nabla g_i \sharp \mu_i$. The implementations of these algorithms are based on published code associated with the papers.

To evaluate the performance of these algorithms, we use the Bures-Wasserstein UVP (Korotin et al., 2021b, Section 5)

$$\text{BW}_2^2\text{–UVP}\left(\nu, \tilde{\nu}\right) \stackrel{\text{def}}{=} 100\frac{\text{BW}_2^2\left(\nu, \tilde{\nu}\right)}{\frac{1}{2}\text{Var}(\tilde{\nu})}\%, \qquad (11)$$

where $\text{BW}_2^2\left(\nu, \tilde{\nu}\right)$ equals

$$\frac{1}{2}\|m_\nu - m_{\tilde{\nu}}\|^2 + \left[\frac{1}{2}\text{Tr}\Sigma_\nu + \frac{1}{2}\text{Tr}\Sigma_{\tilde{\nu}} - \text{Tr}\left(\Sigma_\nu^{\frac{1}{2}}\Sigma_{\tilde{\nu}}\Sigma_\nu^{\frac{1}{2}}\right)^{\frac{1}{2}}\right].$$

Here ν is the estimated barycenter, $\tilde{\nu}$ is the exact barycenter,

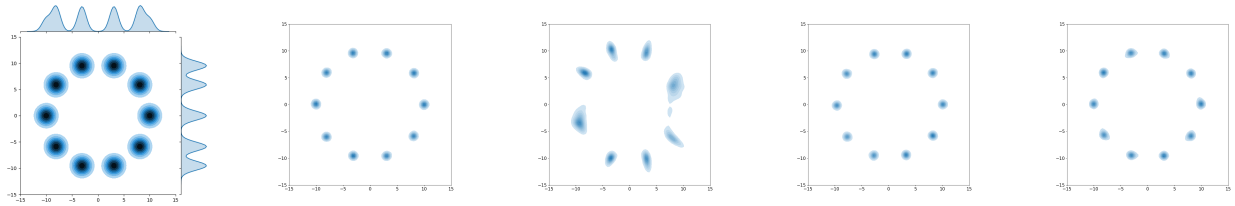

(a) marginal μ_1 (b) NWB (ours) (c) WGAN (d) WGAN-GP (e) W2GN

Figure 3: performance of our algorithm as GAN in single marginal case ($N = 1$): learning Gaussian mixture

and m_ν, Σ_ν are the mean and the convariance of the distribution ν. For barycenter given by pushforward $\nabla g_i \sharp \mu_i$, we report the weighted average of BW_2^2–UVP scores from N marginal distributions: $\sum_{i=1}^N a_i \text{BW}_2^2\text{–UVP}\left(\nabla g_i \sharp \mu_i, \tilde{\nu}\right)$.

Hyper-parameter choice We choose a neural network architecture of $3 \sim 4$ hidden layers of size $1 \sim 2$ times of input dimension in high dim cases and size $16 \sim 32$ in 2D/3D cases, with **PReLU** activation function. We observed that the performance is not sensitive to number of hidden layers, but sensitive to the choice of activation function (ReLU and leaky ReLU do not perform as well as PReLU).

Training time: The training time for our method is almost once to twice longer than of CRWB and CWB due to the inner optimization cycles. The time consumption for CDWB is shorter for small number of samples, as it does not involve training neural networks.

4.1. Learning the Wasserstein Barycenter in 2D and 3D

The qualitative performance of our algorithm in three benchmark examples is depicted in Figure 4. Each example is represented in a row. The first column contains the marginal distributions, and the second and third column contains the learned barycenter through $h\sharp\eta$ and $\nabla g_i \sharp \mu_i$ respectively. It is observed that both representations learn the barycenter qualitatively well, however, representation through $\nabla g_i \sharp \mu_i$ inherits the geometrical properties of the marginal distributions, highlighted with sharp boundaries in the first and second row and pixelated image in the third row. For comparison with CRWB, see Li et al. (2020, Figure 1).

4.2. Scalability with the dimension

Gaussian: We study the performance of our proposed algorithm in learning the barycenter of three Gaussian marginal distributions as dimension grows. The Gaussian marginal distributions have zero mean and a random non-diagonal covariance matrix whose conditional number is less than 10. The exact barycenter of Gaussian distributions is available to serve as the baseline in evaluating the Bures-Wasserstein UVP error criteria (11). The results are displayed in Figure 5. It is observed that the estimation error of NWB and CWB

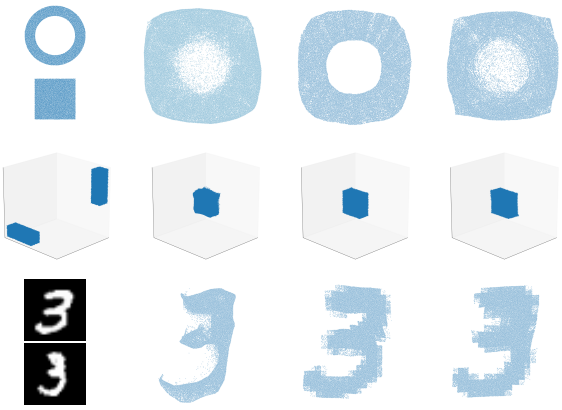

marginals (a) $h\sharp\eta$ (b) $\nabla g_1 \sharp \mu_1$ (c) $\nabla g_2 \sharp \mu_2$

Figure 4: Qualitative results of our algorithm (NWB) in 2D and 3D settings. The first column contains the marginals, and the second and third columns contain the barycenter generated through $h\sharp\eta$ and $\nabla g_i \sharp \mu_i$ respectively. From top to bottom, the marginal distributions are uniformly supported on a ring and a square; two blocks; and white areas in digit images.

exhibit a slow rate of growth with respect to the dimension compared with CDWB and CRWB. The NWB and CWB algorithms are quite comparable in performance, but still different with respect to the optimization landscape. The optimization landscape of CWB is sensitive to the choice of regularization parameters (see Appendix G). We conjecture that the observed error curve of CWB in Figure 5, is due to the effect of regularization terms in distorting the optimization landscape which becomes more severe as dimension grows. Note that the error curve for CRWB contains irregularities and high variance that are probably due to the regularization term.

MNIST: To further investigate the performance of our algorithm in high dimension setting with real dataset, we use the MNIST data set. We consider the task of learning the barycenter of two marginal distributions. The first marginal μ_1 is an empirical distribution of digit 0 samples and the second marginal μ_2 is of digit 1. Each image has 28×28 pixels, yielding a 784-dimensional problem. The result of learning the barycenter is depicted in Figure 6. Both our algorithm NWB and CWB give reasonable results, with

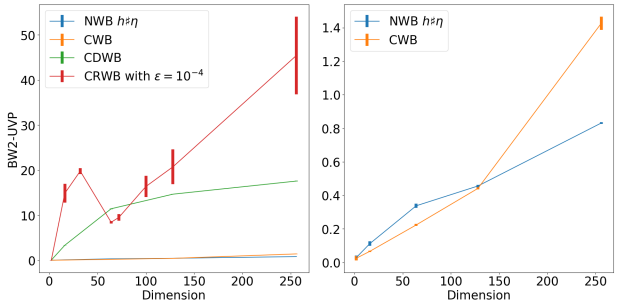

Figure 5: Numerical result for scalability of the error with dimension for estimating barycenter of Gaussian distributions. The error criteria is (11). We generate 10^4 samples from barycenter for NWB, CWB, CRWB algorithms and 1500 samples for CDWB (the maximum number it can generate). The plot on the left includes the results for all four methods and the plot on the right highlights the detailed difference between CWB and NWB.

slightly sharper boundaries in NWB, whereas CRWB does not perform well in this high dimension setting. Note that the images in panel (a) are genuinely new samples generated using the trained generator, while the images in other panels are pushforward of marginal samples.

In order to demonstrate the inner-workings of our algorithm and its ability to learn the structure of barycenter, we implement the following experiment. We generate fresh samples from the barycenter using the generator $h(Z)$, where $Z \sim \mathcal{N}(\mathbf{0}, I)$, and push-forward it through the maps $\nabla f_1(h(Z))$ and $\nabla f_2(h(Z))$. It is expected that through this procedure, we would recover the digits 0 and 1, because ∇f_i represent the optimal transport map from Barycenter to the marginal μ_i (see Remark 1). The experimental result confirms our expectation as shown in Figure 7. This implies that our proposed framework can serve as a generative model, not only for barycenter distribution, but also for the marginal distributions, by taking a random Gaussian random variable as input and output samples from marginal distributions.

4.3. Subset posterior aggregation

MCMC Bayesian inference is often carried out on splitted datasets in big data setting. However, the subset posterior distributions need to be merged into a single posterior to reflect the entire dataset property. This subset posterior aggregation scheme has been shown as an advantageous substitute to the full posterior (Srivastava et al., 2015) (Srivastava et al., 2018). The barycenter of subset posteriors is proved to converge to the full data posterior (Srivastava et al., 2018). Similar to (Li et al., 2020), we consider the Poisson regression for predicting the hourly number of bike hires with predictors such as the season and the weather

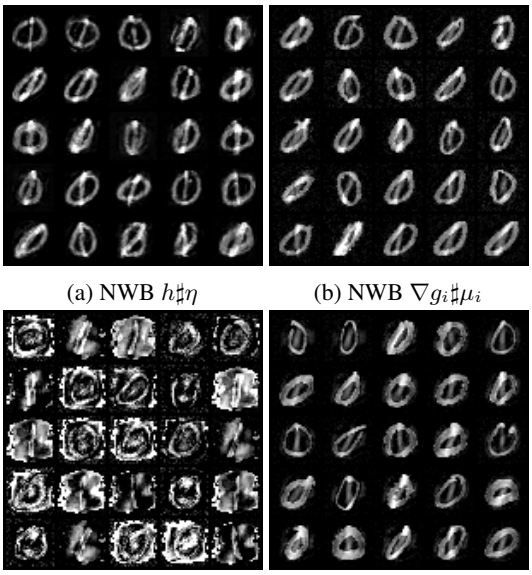

(a) NWB $h\sharp\eta$ (b) NWB $\nabla g_i\sharp\mu_i$

(c) CRWB (d) CWB

Figure 6: Learning the barycenter of MNIST 0 and 1 digits (784-dimensional problem)

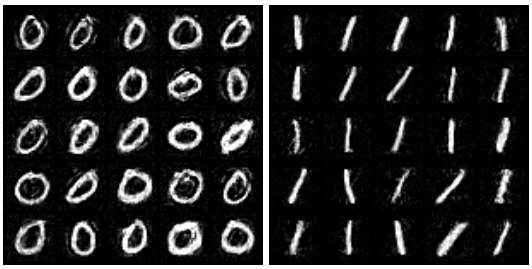

(a) backward to '0' (b) backward to '1'

Figure 7: Generating digit 0 and 1 from random input $Z \sim \mathcal{N}(\mathbf{0}, I)$ using our architecture with the map $\nabla f_i(h(Z))$.

conditions[2]. We consider the posterior on the 8-dimensional coefficients for the Poisson regression model. We randomly split the data into 5 equal-size subsets and simultaneously use the stochastic approximation trick (Minsker et al., 2014) to promise the subset posterior samples do not vary consistently from the full posterior in covariance. We obtain 10^5 samples from each subset posterior using the PyMC3 library (Salvatier et al., 2016).

We use the full posterior samples as the ground truth and report the Bures-Wasserstein UVP to compare the estimated barycenter and the ground truth. The results are shown in Table 1. All methods approach the true barycenter well (UVP $< 1\%$) and the performance of NWB is better than or on par with existing algorithms.

[2] http://archive.ics.uci.edu/ml/datasets/Bike+Sharing+Dataset

Table 1: Comparison of UVP for recovered barycenters in our subset posterior aggregation task

METRIC	NWB $h\sharp\eta$	CDWB	CWB	CRWB
BW_2^2–UVP, %	0.06	0.26	0.07	1.67

4.4. Color palette averaging

Color transfer is a method to change the appearance of a source image according to the color pattern of a target image (Reinhard et al., 2001). Given several images, we can solve for Wasserstein barycenter to aggregate color palettes of images to achieve color transfer among them. Given an RGB image $\mathcal{I}$, its color palette is the empirical distribution $\mu(\mathcal{I}) = \sum_{k=1}^{K} \frac{1}{K}\delta_{p_k}$ where $\{p_k\}$ represents the pixels $\in [0,1]^3$ and δ_{p_k} is the Dirac distribution concentrated on p_k. In our example, each image contains 1980×1024 pixels, so the number of samples for each marginal distribution is more than 2 million. [3].

In Figure 8, the upper panel shows the original images $\{\mathcal{I}_1, \mathcal{I}_2, \mathcal{I}_3\}$, and the bottom panel shows pixel-wise "push-forward" images. Figure 9 shows the RGB cloud to visualize the color palettes of images. In Figure 8, the appearance of the pushforward images are different from the source images thanks to the color averaging: the leaves in the first picture become greener and darker, the sunbeams in the second picture become more red, and the sky in the last picture receives an orange color toning.

Source images $\{\mathcal{I}_i\}$

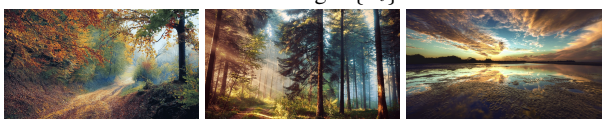

Pushforward images

Figure 8: Qualitative results by pixel-wise pushforward of the source images

4.5. Serving as a Generative Adversarial Model in the one marginal setting

We study the performance of our proposed algorithm in the case of one marginal distribution, where it behaves as a generative adversarial network using the W_2 metric. For comparison, we use WGAN (Arjovsky et al., 2017) and WGAN-GP (Gulrajani et al., 2017), which are based on W_1 metic, and W2GN (Korotin et al., 2021a), which is based on W_2 metric. Note that our goal is not to provide a competitive GAN algorithm, but to demonstrate the ability of our algorithm in performing as GAN.

[3]The pictures are downloaded from https://wallpaperaccess.com/

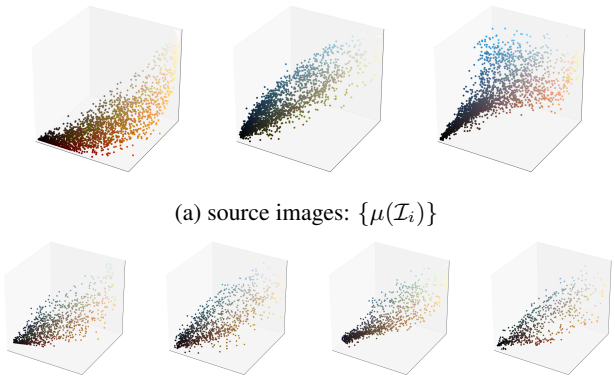

(a) source images: $\{\mu(\mathcal{I}_i)\}$

(b) $\nabla g_1 \sharp \mu(\mathcal{I}_1)$ (c) $\nabla g_2 \sharp \mu(\mathcal{I}_2)$ (d) $\nabla g_3 \sharp \mu(\mathcal{I}_3)$ (e) $h\sharp\eta$

Figure 9: Color palettes of source images and barycenter

We first consider an example of learning a Gaussian mixture model with 10 components shown in Figure 3. It can be seen that NWB avoids mode collapse. We then investigate the performance of our algorithm NWB in learning MNIST digits dataset (784 dim, 60000 sample size). From Figure 10, it is observed that our algorithm could output all the digits from 0 to 9 without mode collapse and the quality is on par with WGAN and WGAN-GP. W2GN seeks an optimal transport map from 784 dim standard Gaussian to MNIST; the generated digits are of poor quality. Note that in Korotin et al. (2021a) W2GN was tested on MNIST dataset but the optimal transport is addressed in the feature/latent space (see Section 5.2, Section C.7 in Korotin et al. (2021a)), which is of much lower dimension than the pixel space (784 dim).

5. Conclusion

During the last decade, many algorithms have been proposed for Wasserstein Barycenter estimation. A majority of these algorithms are designed for discrete setting (either discretization of space or discretization of distribution from samples). There are several algorithms that are designed for semi-discrete setting, in the sense that even though the marginal distributions are continuous, the barycenter computed from the algorithms is supported on finite points. More recently, two algorithms (Korotin et al., 2021b; Li et al., 2020) have been proposed to approximate the barycenter by learning the optimal transport maps from the marginal distributions to the barycenter using samples from the marginal distributions. Compared to all these existing Wasserstein Barycenter estimation algorithm, the NWB algorithm we develop is the only algorithm that gives a continuous representation of the barycenter through a generative model and is capable of generating infinitely many samples from the barycenter.

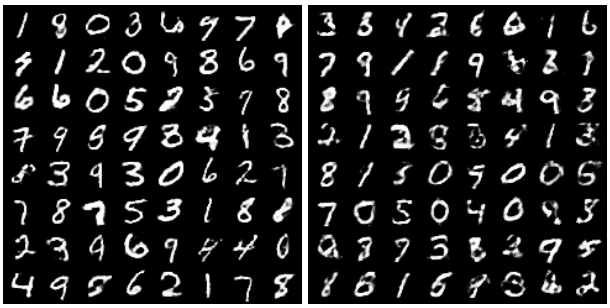

(a) NWB $h\sharp\eta$

(b) WGAN

(c) WGAN-GP

(d) W2GN

Figure 10: Performance of our algorithm as GAN in single marginal case: learning the MNIST digit dataset

Acknowledgments

The authors would like to thank the anonymous reviewers for useful comments. JF and YC are supported in part by grants NSF CAREER ECCS-1942523, NSF CCF-2008513, and NSF CCF-1740776. The authors also thank Qinsheng Zhang for fruitful discussions.

References

Agueh, M. and Carlier, G. Barycenters in the Wasserstein space. *SIAM Journal on Mathematical Analysis*, 43(2): 904–924, 2011.

Altschuler, J. M. and Boix-Adsera, E. Wasserstein barycenters can be computed in polynomial time in fixed dimension. *Journal of Machine Learning Research*, 22(44):1–19, 2021. URL http://jmlr.org/papers/v22/20-588.html.

Álvarez-Esteban, P. C., Del Barrio, E., Cuesta-Albertos, J., and Matrán, C. A fixed-point approach to barycenters in Wasserstein space. *Journal of Mathematical Analysis and Applications*, 441(2):744–762, 2016.

Ambrosio, L., Gigli, N., and Savaré, G. *Gradient flows: in metric spaces and in the space of probability measures*. Springer Science & Business Media, 2008.

Amos, B., Xu, L., and Kolter, J. Z. Input convex neural networks. In *Proceedings of the 34th International Conference on Machine Learning-Volume 70*, pp. 146–155. JMLR. org, 2017.

Anderes, E., Borgwardt, S., and Miller, J. Discrete wasserstein barycenters: Optimal transport for discrete data. *Mathematical Methods of Operations Research*, 84(2): 389–409, 2016.

Andrieu, C., De Freitas, N., Doucet, A., and Jordan, M. I. An introduction to MCMC for machine learning. *Machine learning*, 50(1-2):5–43, 2003.

Arjovsky, M., Chintala, S., and Bottou, L. Wasserstein generative adversarial networks. In Precup, D. and Teh, Y. W. (eds.), *Proceedings of the 34th International Conference on Machine Learning*, volume 70 of *Proceedings of Machine Learning Research*, pp. 214–223, International Convention Centre, Sydney, Australia, 06–11 Aug 2017. PMLR.

Benamou, J.-D., Carlier, G., Cuturi, M., Nenna, L., and Peyré, G. Iterative Bregman projections for regularized transportation problems. *SIAM Journal on Scientific Computing*, 37(2):A1111–A1138, 2015.

Bonneel, N., Van De Panne, M., Paris, S., and Heidrich, W. Displacement interpolation using lagrangian mass transport. In *Proceedings of the 2011 SIGGRAPH Asia Conference*, pp. 1–12, 2011.

Chen, Y., Georgiou, T. T., and Tannenbaum, A. Optimal transport for gaussian mixture models. *IEEE Access*, 7: 6269–6278, 2018a.

Chen, Y., Shi, Y., and Zhang, B. Optimal control via neural networks: A convex approach, 2018b.

Chewi, S., Maunu, T., Rigollet, P., and Stromme, A. J. Gradient descent algorithms for bures-wasserstein barycenters. *arXiv preprint arXiv:2001.01700*, 2020.

Claici, S., Chien, E., and Solomon, J. Stochastic Wasserstein barycenters. *arXiv preprint arXiv:1802.05757*, 2018.

Cuturi, M. Sinkhorn distances: Lightspeed computation of optimal transport. In *Advances in neural information processing systems*, pp. 2292–2300, 2013.

Cuturi, M. and Doucet, A. Fast computation of Wasserstein barycenters. 2014.

Elvander, F., Haasler, I., Jakobsson, A., and Karlsson, J. Tracking and sensor fusion in direction of arrival estimation using optimal mass transport. In *2018 26th European Signal Processing Conference (EUSIPCO)*, pp. 1617–1621. IEEE, 2018.

Flamary, R. and Courty, N. Pot python optimal transport library, 2017. URL https://pythonot.github.io/.

Genevay, A., Cuturi, M., Peyré, G., and Bach, F. Stochastic optimization for large-scale optimal transport. In *Advances in neural information processing systems*, pp. 3440–3448, 2016.

Genevay, A., Peyre, G., and Cuturi, M. Learning generative models with sinkhorn divergences. In Storkey, A. and Perez-Cruz, F. (eds.), *Proceedings of the Twenty-First International Conference on Artificial Intelligence and Statistics*, volume 84 of *Proceedings of Machine Learning Research*, pp. 1608–1617. PMLR, 09–11 Apr 2018. URL http://proceedings.mlr.press/v84/genevay18a.html.

Goodfellow, I., Pouget-Abadie, J., Mirza, M., Xu, B., Warde-Farley, D., Ozair, S., Courville, A., and Bengio, Y. Generative adversarial nets. In *Advances in neural information processing systems*, pp. 2672–2680, 2014.

Gulrajani, I., Ahmed, F., Arjovsky, M., Dumoulin, V., and Courville, A. C. Improved training of wasserstein gans. *Advances in neural information processing systems*, 30: 5767–5777, 2017.

He, K., Zhang, X., Ren, S., and Sun, J. Delving deep into rectifiers: Surpassing human-level performance on imagenet classification. In *Proceedings of the IEEE international conference on computer vision*, pp. 1026–1034, 2015.

Jiang, X., Ning, L., and Georgiou, T. T. Distances and Riemannian metrics for multivariate spectral densities. *IEEE Transactions on Automatic Control*, 57(7):1723–1735, 2012.

Korotin, A. Wasserstein-2 generative networks, 2020. URL https://github.com/iamalexkorotin/Wasserstein2GenerativeNetworks.

Korotin, A., Egiazarian, V., Asadulaev, A., Safin, A., and Burnaev, E. Wasserstein-2 generative networks. In *International Conference on Learning Representations*, 2021a. URL https://openreview.net/forum?id=bEoxzW_EXsa.

Korotin, A., Li, L., Solomon, J., and Burnaev, E. Continuous wasserstein-2 barycenter estimation without minimax optimization. In *International Conference on Learning Representations*, 2021b. URL https://openreview.net/forum?id=3tFAs5E-Pe.

Kuang, M. and Tabak, E. G. Sample-based optimal transport and barycenter problems. *Communications on Pure and Applied Mathematics*, 72(8):1581–1630, 2019.

Leygonie, J., She, J., Almahairi, A., Rajeswar, S., and Courville, A. Adversarial computation of optimal transport maps. *arXiv preprint arXiv:1906.09691*, 2019.

Li, L. Cwb, 2020. URL https://github.com/lingxiaoli94/CWB.

Li, L., Genevay, A., Yurochkin, M., and Solomon, J. M. Continuous regularized wasserstein barycenters. *Advances in Neural Information Processing Systems*, 33, 2020.

Linder-Norén, E. Pytorch-gan, 2018. URL https://github.com/eriklindernoren/PyTorch-GAN.

Liu, H., Xianfeng, G., and Samaras, D. A two-step computation of the exact gan wasserstein distance. In *International Conference on Machine Learning*, pp. 3159–3168, 2018.

Luise, G., Salzo, S., Pontil, M., and Ciliberto, C. Sinkhorn barycenters with free support via frank-wolfe algorithm. In Wallach, H., Larochelle, H., Beygelzimer, A., d'Alché-Buc, F., Fox, E., and Garnett, R. (eds.), *Advances in Neural Information Processing Systems*, volume 32. Curran Associates, Inc., 2019. URL https://proceedings.neurips.cc/paper/2019/file/9f96f36b7aae3b1ff847c26ac94c604e-Paper.pdf.

Makkuva, A., Taghvaei, A., Oh, S., and Lee, J. Optimal transport mapping via input convex neural networks. In *International Conference on Machine Learning*, pp. 6672–6681. PMLR, 2020.

Mi, L., Yu, T., Bento, J., Zhang, W., Li, B., and Wang, Y. Variational Wasserstein barycenters for geometric clustering. *arXiv preprint arXiv:2002.10543*, 2020.

Minsker, S., Srivastava, S., Lin, L., and Dunson, D. Scalable and robust bayesian inference via the median posterior. In *International conference on machine learning*, pp. 1656–1664, 2014.

Peyré, G., Cuturi, M., et al. Computational optimal transport. *Foundations and Trends® in Machine Learning*, 11(5-6): 355–607, 2019.

Rabin, J., Peyré, G., Delon, J., and Bernot, M. Wasserstein barycenter and its application to texture mixing. In *International Conference on Scale Space and Variational Methods in Computer Vision*, pp. 435–446. Springer, 2011.

Reinhard, E., Adhikhmin, M., Gooch, B., and Shirley, P. Color transfer between images. *IEEE Computer graphics and applications*, 21(5):34–41, 2001.

Rockafellar, R. T. *Convex analysis*. Number 28. Princeton university press, 1970.

Salimans, T., Zhang, H., Radford, A., and Metaxas, D. Improving GANs using optimal transport. In *International Conference on Learning Representations*, 2018. URL https://openreview.net/forum?id=rkQkBnJAb.

Salvatier, J., Wiecki, T. V., and Fonnesbeck, C. Probabilistic programming in python using pymc3. *PeerJ Computer Science*, 2:e55, 2016.

Seguy, V., Damodaran, B. B., Flamary, R., Courty, N., Rolet, A., and Blondel, M. Large-scale optimal transport and mapping estimation. *arXiv preprint arXiv:1711.02283*, 2017.

Solomon, J., De Goes, F., Peyré, G., Cuturi, M., Butscher, A., Nguyen, A., Du, T., and Guibas, L. Convolutional Wasserstein distances: Efficient optimal transportation on geometric domains. *ACM Transactions on Graphics (TOG)*, 34(4):1–11, 2015.

Srivastava, S., Cevher, V., Dinh, Q., and Dunson, D. WASP: Scalable Bayes via barycenters of subset posteriors. In *Artificial Intelligence and Statistics*, pp. 912–920, 2015.

Srivastava, S., Li, C., and Dunson, D. B. Scalable Bayes via barycenter in Wasserstein space. *The Journal of Machine Learning Research*, 19(1):312–346, 2018.

Staib, M., Claici, S., Solomon, J. M., and Jegelka, S. Parallel streaming Wasserstein barycenters. In *Advances in Neural Information Processing Systems*, pp. 2647–2658, 2017.

Taghvaei, A. and Jalali, A. 2-wasserstein approximation via restricted convex potentials with application to improved training for gans. *arXiv preprint arXiv:1902.07197*, 2019.

Villani, C. *Topics in optimal transportation*. Number 58. American Mathematical Soc., 2003.

Xie, Y., Chen, M., Jiang, H., Zhao, T., and Zha, H. On scalable and efficient computation of large scale optimal transport. *arXiv preprint arXiv:1905.00158*, 2019.

Yang, H. and Tabak, E. G. Clustering, factor discovery and optimal transport. *arXiv preprint arXiv:1902.10288*, 2019.